

Superconducting state in $Ba_{(1-x)}Sr_xNi_2As_2$ near the quantum critical point

Chengfeng Yu(余承峰), Zongyuan Zhang(张宗源), Linxing Song(宋林兴), Yanwei Wu(吴彦玮), Xiaoqiu Yuan(袁小秋), Jie Hou(侯杰), Yubing Tu(涂玉兵), Xingyuan Hou(侯兴元), Shiliang Li(李世亮), and Lei Shan(单磊),
Citation: Chin. Phys. B, 2024, 33 (**6**): 066802. DOI: 10.1088/1674-1056/ad334a
Journal homepage: http://cpb.iphy.ac.cn; http://iopscience.iop.org/cpb

What follows is a list of articles you may be interested in

Microscopic growth mechanism and edge states of monolayer 1T'-$MoTe_2$

Haipeng Zhao(赵海鹏), Yin Liu(刘隐), Shengguo Yang(杨胜国), Chenfang Lin(林陈昉), Mingxing Chen(陈明星), Kai Braun, Xinyi Luo(罗心仪), Siyu Li(李思宇), Anlian Pan(潘安练), and Xiao Wang(王笑)
Chin. Phys. B, 2024, 33 (**4**): 046801. DOI: 10.1088/1674-1056/ad16d5

Growth and characterization of Bi(110)/$CrTe_2$ heterostructures: Exploring interplay between magnetism and topology

Zhenyu Yuan(袁震宇), Fazhi Yang(杨发枝), Baiqing Lv(吕佰晴), Yaobo Huang(黄耀波), Tian Qian(钱天), Jinpeng Xu(徐金朋), and Hong Ding(丁洪)
Chin. Phys. B, 2024, 33 (**2**): 026802. DOI: 10.1088/1674-1056/ad082a

Adsorption structure of macrocyclic energetic molecule DOATF on Au(111)

Xiao Chang(常霄), Li Huang(黄立), Yixuan Gao(高艺璇), Changjiang Yu(于长江), Yun Cao(曹云), Long Lv(吕龙), Xiao Lin(林晓), Shixuan Du(杜世萱), and Hong-Jun Gao(高鸿钧)
Chin. Phys. B, 2023, 32 (**9**): 096802. DOI: 10.1088/1674-1056/acda84

Manipulating charge density wave state in kagome compound RbV_3Sb_5

Yu-Xin Meng(孟雨欣), Cheng-Long Xue(薛成龙), Li-Guo Dou(窦立国), Wei-Min Zhao(赵伟民), Qi-Wei Wang(汪琪玮), Yong-Jie Xu(徐永杰), Xiangqi Liu(刘祥麒), Wei Xia(夏威), Yanfeng Guo(郭艳峰), and Shao-Chun Li(李绍春)
Chin. Phys. B, 2023, 32 (**9**): 096801. DOI: 10.1088/1674-1056/acd8b1

Critical behavior in the epitaxial growth of two-dimensional tellurium films on $SrTiO_3$ (001) substrates

Haimin Zhang(张海民), Dezhi Song(宋德志), Fuyang Huang(黄扶旸), Jun Zhang(仉君), and Ye-Ping Jiang(蒋烨平)
Chin. Phys. B, 2023, 32 (**6**): 066802. DOI: 10.1088/1674-1056/acc80d

---

Superconducting state in $Ba_{(1-x)}Sr_xNi_2As_2$ near the quantum critical point

Chengfeng Yu(余承峰)[1,2], Zongyuan Zhang(张宗源)[1,2,†], Linxing Song(宋林兴)[3,4], Yanwei Wu(吴彦玮)[1,2], Xiaoqiu Yuan(袁小秋)[1,2], Jie Hou(侯杰)[1,2], Yubing Tu(涂玉兵)[1,2], Xingyuan Hou(侯兴元)[1,2], Shiliang Li(李世亮)[3,4,5,‡], and Lei Shan(单磊)[1,2,§]

[1] *Information Materials and Intelligent Sensing Laboratory of Anhui Province, Institutes of Physical Science and Information Technology, Anhui University, Hefei* 230601, *China*

[2] *Key Laboratory of Structure and Functional Regulation of Hybrid Materials (Anhui University), Ministry of Education, Hefei* 230601, *China*

[3] *Beijing National Laboratory for Condensed Matter Physics, Institute of Physics, Chinese Academy of Sciences, Beijing* 100190, *China*

[4] *School of Physical Sciences, University of Chinese Academy of Sciences, Beijing* 100190, *China*

[5] *Songshan Lake Materials Laboratory, Dongguan* 523808, *China*

(Received 10 January 2024; revised manuscript received 18 February 2024; accepted manuscript online 13 March 2024)

In the phase diagram of the nickel-based superconductor $Ba_{1-x}Sr_xNi_2As_2$, T_c has been found to be enhanced sixfold near the quantum critical point (QCP) $x = 0.71$ compared with the parent compound. However, the mechanism is still under debate. Here, we report a detailed investigation of the superconducting properties near the QCP ($x \approx 0.7$) by utilizing scanning tunneling microscopy and spectroscopy. The temperature-dependent superconducting gap and magnetic vortex state were obtained and analyzed in the framework of the Bardeen–Cooper–Schrieffer model. The ideal isotropic s-wave superconducting gap excludes the long-speculated nematic fluctuations while preferring strong electron–phonon coupling as the mechanism for T_c enhancement near the QCP. The lower than expected gap ratio of $\Delta/(k_BT_c)$ is rooted in the fact that $Ba_{1-x}Sr_xNi_2As_2$ falls into the dirty limit with a serious pair breaking effect similar to the parent compound.

Keywords: nickel-based superconductor, electron–phonon coupling, dirty limit, scanning tunneling microscopy/spectroscopy

PACS: 74.25.–q, 07.79.Fc, 74.55.+v, 74.25.Uv **DOI:** 10.1088/1674-1056/ad334a

The phenomenon of superconductivity is often accompanied by other novel charge orders, such as charge density waves (CDWs), spin density waves (SDWs) and nematic phases.[1–3] $BaNi_2As_2$ does not exhibit magnetic order[4] but possesses rich charge orders,[5–7] making it an excellent platform for studying the interaction between charge orders and superconductivity. Although $BaNi_2As_2$ has a structure similar to that of the 122-type iron-based superconductor $BaFe_2As_2$,[8–10] and an electronic phase diagram showing doping-induced T_c variation,[5–7,11,12] there are significant differences between them in band structures and correlation effects.[13] Compared with the unconventional superconducting behavior of iron-based superconductors, $BaNi_2As_2$ is a weakly coupled conventional s-wave superconductor with a very low T_c (0.7 K).[14] The electron–phonon coupling (EPC) pairing mechanism has also been verified by density functional theory (DFT) calculations.[15]

By doping Sr into $BaNi_2As_2$, the obtained $Ba_{1-x}Sr_xNi_2As_2$ shows a quantum critical point (QCP; $x_c = 0.71$) in the phase diagram where the inherent nematic order in the parent compound vanishes, whereas the superconducting critical temperature increases by a factor of six.[6] Subsequent theoretical studies suggested that the nematic fluctuations near the QCP are responsible for such a significant enhancement of T_c. According to this picture, superconducting gap anisotropy is predicted to be promoted by nematic fluctuations, which are observable in tunneling spectroscopy.[16,17] However, recent neutron scattering studies indicate that the superconductivity enhancement may merely originate from phonon softening in the doped samples rather than nematic fluctuations.[18] Therefore, a detailed investigation of the superconducting properties near the QCP, especially the determination of the gap structure, is essential to resolve this debate. Up to now, research into the superconducting gap around the QCP remains insufficient. Specific heat experiments have only been carried out down to approximately 2 K,[6] and could not accurately determine the gap anisotropy. On the other hand, recent scanning tunneling microscopy and spectroscopy (STM/STS) experiments were performed on undoped and underdoped samples ($x = 0.5$)[19] with $T_c \approx 1.4$ K and a very low upper critical field ($H_{c2} < 0.1$ T), which is far from the QCP.

In this work, we studied the superconducting properties of $Ba_{0.3}Sr_{0.7}Ni_2As_2$ using low-temperature STM/STS. A spatially uniform superconducting gap was observed, ev-

†Corresponding author. E-mail: zongyuanzhang@ahu.edu.cn
‡Corresponding author. E-mail: slli@iphy.ac.cn
§Corresponding author. E-mail: lshan@ahu.edu.cn

© 2024 Chinese Physical Society and IOP Publishing Ltd

idencing a conventional s-wave superconductivity near the QCP of $Ba_{1-x}Sr_xNi_2As_2$. By fitting the tunneling spectra to the Bardeen–Cooper–Schrieffer (BCS) formula, an ideal isotropic superconducting gap was determined, contrary to the theories predicting nematic fluctuation-enhanced superconductivity.[16,17] The obtained gap ratio of $\Delta/(k_BT_c)$ and the coherence length suggest that $Ba_{0.3}Sr_{0.7}Ni_2As_2$ is a strong coupling superconductor in the dirty limit, supporting the scenario of strong EPC-enhanced superconductivity derived from neutron experiments.[18]

Single crystals of $Ba_{0.3}Sr_{0.7}Ni_2As_2$ were grown by the self-flux method as reported previously.[6] STM/STS experiments were conducted using a low-temperature scanning tunneling microscope (Unisoku USM-1300). The single crystals were cleaved in ultra-high vacuum (UHV) at 77 K and subsequently transferred to the scanning tunneling microscope head, which was precooled to around 4 K. Electrochemically etched tungsten tips were utilized in the experiments. The tips were cleaned by electron beam heating to remove surface oxides, and their states were calibrated *in situ* on an Au (111) surface. Topographic images were acquired in constant-current mode, while tunneling spectra were collected using lock-in amplification with a modulation frequency of 973.127 Hz and a modulation voltage $V_{mod} = 0.05$ mV, unless otherwise stated.

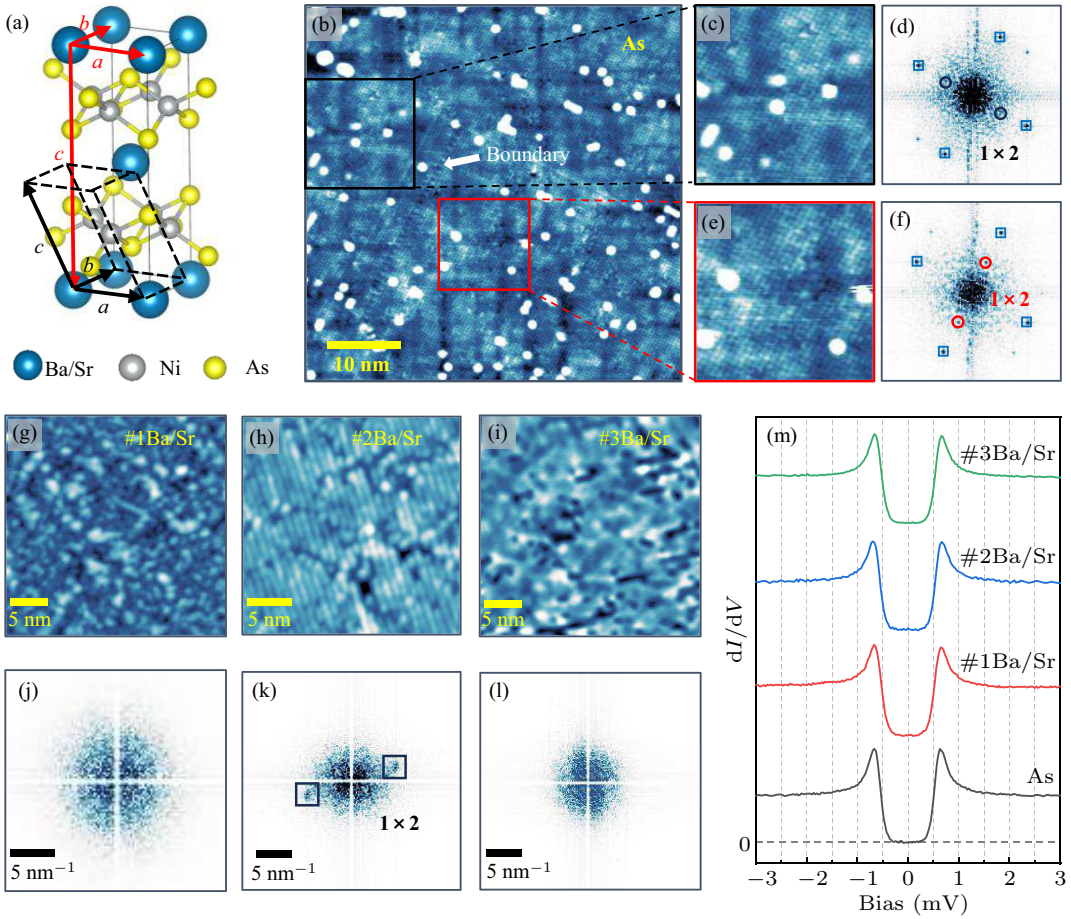


Fig. 1. Surface morphology of $Ba_{1-x}Sr_xNi_2As_2$. (a) Crystal structure of $Ba_{1-x}Sr_xNi_2As_2$ in the tetragonal (red lines) and triclinic (black lines) phases. (b) Constant-current STM topography of the NiAs surface ($V_s = -100$ mV, $I = 100$ pA). (c)–(f) Zoom-in STM topographies of the two sides of the boundary and their corresponding fast Fourier transform (FFT) images. (g)–(i) Surface morphologies of three types of Ba/Sr faces ($V_s = -600$ mV, $I = 20$ pA, $V_s = -100$ mV, $I = 20$ pA, $V_s = -500$ mV, $I = 50$ pA, respectively). (j)–(l) Corresponding FFT images for (g)–(i). (m) Superconducting spectra on four types of surfaces.

As shown in Fig. 1(a), $BaNi_2As_2$ has a tetragonal $I4/mmm$ symmetry at room temperature and undergoes a first-order structural transition from tetragonal to triclinic crystal structure at $T_s = 136$ K.[20,21] It is generally accepted that the interactions between adjacent As and Ba layers are the weakest in this type of compound, leading to two types of surfaces formed by As or Ba/Sr atoms after cleavage, as observed in this work. Figure 1(b) displays a typical atomic-resolution topographic image of the exposed As surface from $Ba_{0.3}Sr_{0.7}Ni_2As_2$, showing a 1×2 superstructure without CDW order similar to that of $Ba_{0.5}Sr_{0.5}Ni_2As_2$.[19] In addition, the superstructure was found to be separated into distinct domains by boundary-like features, and two adjacent domains with perpendicular orientations are depicted in Figs. 1(c)–1(f).[19]

In general, the local density of states (LDOS) detected by STS depends on the cleaved termination surface.[22,23] On $Ba_{0.3}Sr_{0.7}Ni_2As_2$, four types of surfaces can be obtained after

cleavage; these are recognized by different Ba/Sr atomic coverages. As mentioned above, Fig. 1(b) shows an As surface containing only some isolated Ba/Sr adatoms. Figures 1(g)–1(i) display termination surfaces covered by a large number of scattered Ba/Sr atoms, an ordered 1×2 Ba/Sr superstructure and a compact Ba/Sr plane, respectively. The corresponding fast Fourier transform images are given in Figs. 1(j)–1(l), in which only the ordered 1×2 Ba/Sr superstructure contributes two clear wave vectors. Unlike the 1×3 CDW observed on the Ba surface in the parent compound,[19] the superstructure observed here should be due to the insufficiency of Ba/Sr atoms, similar to the half-Cs surface in CsV_3Sb_5.[22] It is interesting to find that the tunneling spectra randomly taken on the four types of surfaces are almost identical, as shown in Fig. 1(m). Furthermore, the superconducting gap estimated by the coherence peaks on the spectra is remarkably uniform across the entire surface, as shown in Figs. 2(d)–2(f), unaffected by the structural modulation (Fig. 2(a)), step edges (Fig. 2(b)) or the distribution of Ba/Sr atoms (Fig. 2(c)). This indicates a relatively large superconducting coherence length as expected in conventional superconductors. It is thus concluded that $Ba_{1-x}Sr_xNi_2As_2$ hosts bulk superconductivity, and the measured spectra reflect its bulk properties.

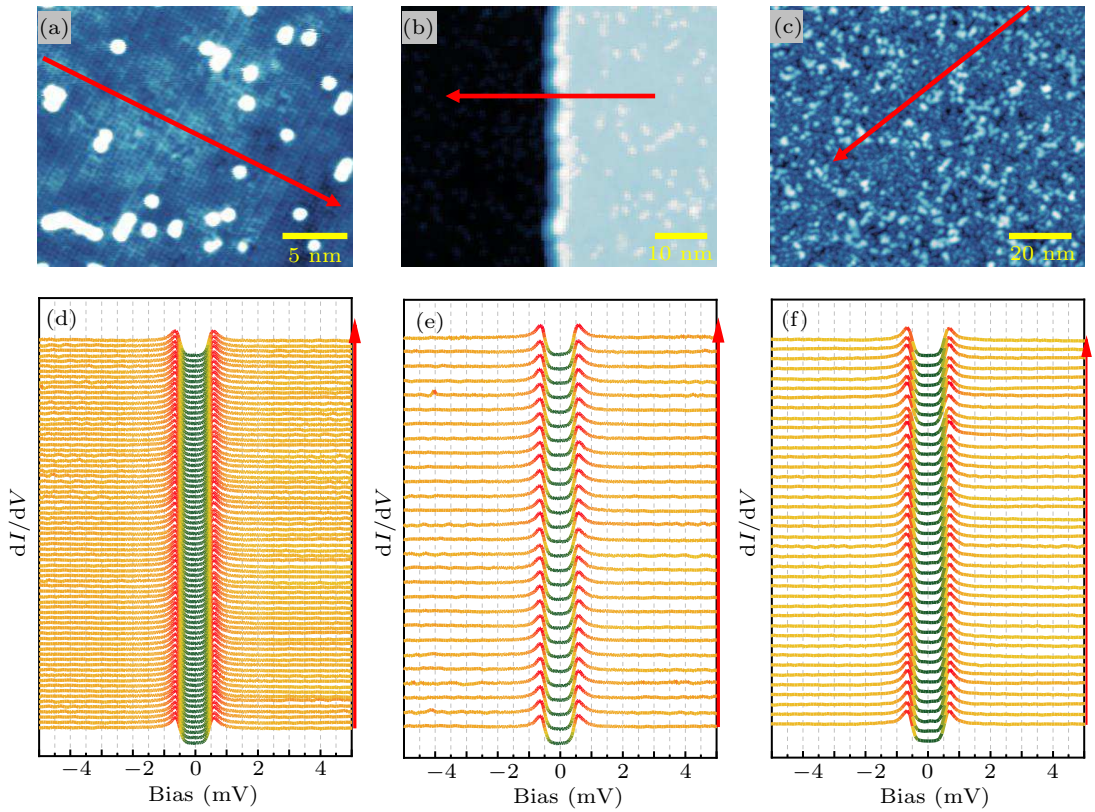


Fig. 2. Spatial uniformity of superconductivity. (a) Constant-current STM topography of the NiAs surface ($V_s = -100$ mV, $I = 100$ pA). (b) Constant-current STM topography of the NiAs surface steps ($V_s = -100$ mV, $I = 15$ pA). (c) Constant-current STM topography of the Ba/Sr surface ($V_s = -100$ mV, $I = 15$ pA). (d)–(f) Spatially resolved spectra measured along the red arrowed lines in (a)–(c), with $V_{mod} = 0.1$ mV.

In order to determine the superconducting order parameter more accurately, temperature-dependent tunneling spectra were measured, as shown in Fig. 3(a). With increasing temperature, the superconducting coherence peaks are gradually suppressed and the energy gap is gradually filled in. As shown in Fig. 3(b), the extracted temperature dependence of zero-bias conductance follows the rule of conventional superconductors, from which the superconducting transition temperature can be determined to be $T_c \approx 3.42$ K, consistent with the value from transport experiments.[6] Figure 3(c) displays the fitting results using the Dynes model[24] with an isotropic s-wave gap. The determined broadening parameter Γ is less than 0.02 meV, indicating quite a long lifetime of the superconducting quasiparticles. The obtained temperature dependence of the superconducting gap is in good agreement with the BCS law with a gap ratio of $\Delta/(k_B T_c) = 1.93$, as presented in Fig. 3(d). All these results demonstrate that $Ba_{0.3}Sr_{0.7}Ni_2As_2$ is a conventional isotropic s-wave superconductor. The perfect gap isotropy revealed here is difficult to reconcile with the mechanism of nematic fluctuation-enhanced superconductivity, as mentioned above.[16,17] Alternatively, the mechanism based on doping-induced phonon softening and a larger EPC coefficient conforms with the isotropic gap function observed here. However, the moderated gap ratio of 1.93, close to the weak coupling value of 1.75, does not seem strong enough to account for the sixfold enhancement of T_c caused by doping. Furthermore, strong coupling between electrons and bosonic modes typically manifests in tunneling spectra as hump–dip features

outside the superconducting gap, which is more distinct in the second derivative of tunneling current (d^2I/dV^2) at the energies of bosonic modes.[25–29] As shown in Fig. 3(e), no features are visible outside the gap in the spectra of d^2I/dV^2. To clarify this issue, it is necessary to compare the results for $Ba_{0.3}Sr_{0.7}Ni_2As_2$ with those for the parent compound. It has been noted that $BaNi_2As_2$ has a gap ratio of 1.61, smaller than the weak coupling value of 1.75, which has been ascribed to the fact that $BaNi_2As_2$ samples are in the dirty limit, as proved by thermal conductivity data.[14] Since the doped sample is not expected to be cleaner than the parent compound, the properties of $Ba_{0.3}Sr_{0.7}Ni_2As_2$ should also be limited by the dirty limit. Such a regime naturally explains the lower gap ratio than expected and the disappearance of electron–boson coupling features[30] observed here in $Ba_{0.3}Sr_{0.7}Ni_2As_2$. Thus, information about the coherence length and mean free path in $Ba_{0.3}Sr_{0.7}Ni_2As_2$ is necessary to judge if it falls into a dirty limit, which can be obtained from the measurements of spatially dependent spectra/LDOS in magnetic fields.

Figure 4(a) displays tunneling spectra measured under various magnetic fields from 0 to the upper critical field $H_{c2} \sim 1.2$ T. To accurately determine H_{c2}, spectra were taken at locations far from the vortex core. Since superconductivity is suppressed upon approaching vortex cores, images of vortices could be obtained by mapping zero-bias conductance (ZBC) in a magnetic field, as illustrated in Figs. 4(b) and 4(c) for 0.1 T and 0.6 T, respectively. Figure 4(d) shows a series of spectra taken along the arrowed line spanning a vortex and a superconducting region. Although superconductivity vanishes at the vortex center, no apparent Caroli–de Gennes–Matricon bound states[31,32] were observed, which are usually manifested as a zero-bias conductance peak (ZBCP) in the tunneling spectra. The broadening of the ZBCP into a featureless normal background is generally attributed to strong scattering in the dirty limit.[33–35] To verify this, the Ginzburg–Landau coherence length ξ_{GL} was estimated by fitting the radially dependent ZBC to an exponential formula. As illustrated in the inset of Fig. 4(e), a coherence length of $\xi_{GL} \approx 20 \pm 1.5$ nm was obtained, which is close to the value derived from H_{c2}, i.e., $\xi_{GL} = [\frac{\Phi_0}{2\pi H_{c2}(0)}]^{1/2} = 16.5$ nm (where Φ_0 is the flux quantum and $H_{c2}(0)$ is the upper critical field). Using the same fitting method, the coherence lengths for various magnetic fields were obtained, as presented in Fig. 4(e). It can be seen that the ξ–H relationship significantly deviates from that of a clean BCS superconductor (Fig. 4(e)), tending to the case of the dirty limit.[36]

Since doping of Sr into $BaNi_2As_2$ does not cause significant changes in the band structure and Fermi surface topology[37] it is reasonable to estimate the characteristic lengths of $Ba_{0.3}Sr_{0.7}Ni_2As_2$ adopting the Fermi velocity of the parent compound $v_F = 2.96 \times 10^5$ m/s.[14] So, in the three-dimensional case, the BCS coherence length could be calculated with the formula $\xi_{BCS} = 0.276\frac{\hbar v_F}{k_B T_c} = 181.7$ nm,[36] which is much larger than the value of ξ_{GL} determined above. This, once again, demonstrates that $Ba_{0.3}Sr_{0.7}Ni_2As_2$ is located in the dirty limit. By assigning the determined ξ_{GL} and ξ_{BCS} into the dirty-limit relation $\xi_{GL} = 0.855(\xi_{BCS} l)^{1/2}$,[38] a mean free path of $l \approx 2$ nm can be obtained. Since Sr dopants serve as scattering centers, the fact that the mean free path of $Ba_{0.3}Sr_{0.7}Ni_2As_2$ is shorter than that of $BaNi_2As_2$ ($l \approx 7$ nm) is reasonable.

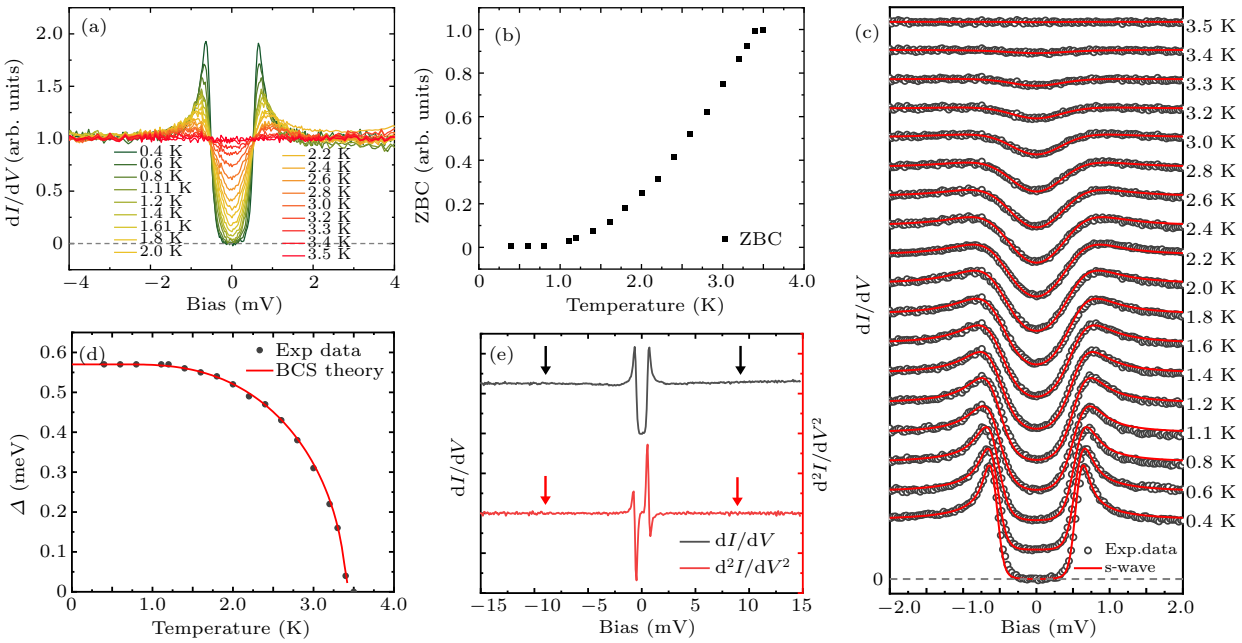


Fig. 3. Superconducting gap structure. (a) Evolution of the superconducting gap with temperature. (b) Variation of zero-bias conductance (ZBC) with temperature. (c) Fitting of the isotropic s-wave function using the Dynes model. (d) Temperature dependence of the superconducting gap, in which the red line follows the BCS theory. (e) Superconducting spectrum and the corresponding second derivative of tunneling current over an energy range of ±15 meV (the marked positions in the figure indicate the potential locations where the bosonic mode may appear).

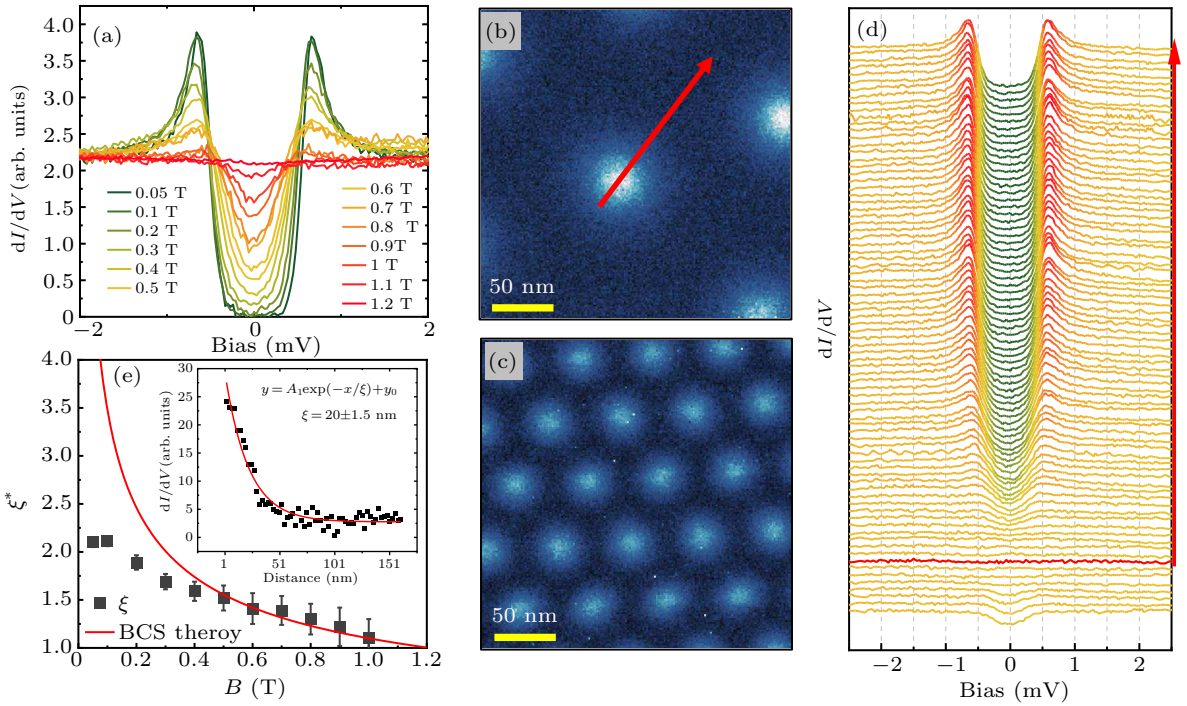


Fig. 4. Superconductivity under a magnetic field. (a) Evolution of the superconducting gap with magnetic field. (b), (c) Zero-energy state density map at magnetic fields of 0.1 T and 0.6 T, respectively ($V_{\rm mod} = 0.15$ mV). (d) Spatial evolution of the spectra across the vortex center along the path indicated in (b) (the red line is the spectrum of the vortex center). (e) Evolution of the coherence length with magnetic fields ($\xi^* = \xi(H)/\xi(H_{c2})$), with the inset showing the exponential fit of the zero-energy state density from the vortex center to the normal region at 0.1 T using a function $y = A_1 \exp(-x/\xi) + y_0$.

In summary, we have utilized scanning tunneling microscopy and spectroscopy to investigate the surface morphology and superconducting properties of $Ba_{1-x}Sr_xNi_2As_2$ near the quantum critical point (QCP) ($x \approx 0.7$). It was found that Sr dopants break long-range structural modulation in the As surface, while keeping the spatial homogeneity of the superconducting gap. The gap function was determined to be completely isotropic, leading to the solid conclusion that the six-fold enhancement of superconducting critical temperature induced by Sr doping near the QCP is not dominated by nematic fluctuations. The much larger gap ratio of $Ba_{0.3}Sr_{0.7}Ni_2As_2$ compared with that of the parent compound can be well understood by the phonon softening-induced strong electron–phonon coupling in the former, which should also be responsible for the remarkable enhancement of superconductivity. These results provide a deeper understanding of the superconducting properties of the $Ba_{1-x}Sr_xNi_2As_2$ system and resolve the controversy about the mechanism of superconductivity enhancement at the QCP.

Acknowledgements

Project supported by the National Key R&D Program of China (Grant Nos. 2022YFA1403203, 2022YFA1403400, and 2021YFA1400400), the Innovation Program for Quantum Science and Technology (Grant No. 2021ZD0302802), the National Natural Science Foundation of China (Grant Nos. 12074002, 12104004, 12204008, and 12374133), the Chinese Academy of Sciences (Grant Nos. XDB33000000 and GJTD-2020-01), and the Major Basic Program of Natural Science Foundation of Shandong Province (Grant No. ZR2021ZD01).

References

[1] Cao Y, Rodan-Legrain D, Park J M, Yuan N F, Watanabe K, Taniguchi T, Fernandes R M, Fu L and Jarillo-Herrero P 2021 *Science* **372** 264
[2] Davis J S and Lee D H 2013 *Proc. Natl. Acad. Sci. USA* **110** 17623
[3] Fradkin E, Kivelson S A and Tranquada J M 2015 *Rev. Mod. Phys.* **87** 457
[4] Kothapalli K, Ronning F, Bauer E, Schultz A and Nakotte H 2010 *J. Phys. Conf. Ser.* **251** 012010
[5] Frachet M, Wiecki P, Lacmann T, Souliou S, Willa K, Meingast C, Merz M, Haghighirad A A, Le Tacon M and Böhmer A 2022 *npj Quantum Mater.* **7** 115
[6] Eckberg C C D J, Metz T, Collini J, Hodovanets H, Drye T, Zavalij P, Christensen M H, Fernandes R M, Lee S, Abbamonte P, Jeffrey W L and Paglione J 2020 *Nat. Phys.* **16** 346
[7] Lee S, Collini J, Sun S X L, Mitrano M, Guo X, Eckberg C, Paglione J, Fradkin E and Abbamonte P 2021 *Phys. Rev. Lett.* **127** 027602
[8] Sefat A S, McGuire M A, Jin R, Sales B C, Mandrus D, Ronning F, Bauer E and Mozharivskyj Y 2009 *Phys. Rev. B* **79** 094508
[9] Li L, Luo Y, Wang Q, Chen H, Ren Z, Tao Q, Li Y, Lin X, He M and Zhu Z 2009 *New J. Phys.* **11** 025008
[10] Johrendt D and Pöttgen R 2009 *Physica C* **469** 332
[11] Lee S, De La Penã G, Sun S X L, Mitrano M, Fang Y, Jang H, Lee J S, Eckberg C, Campbell D and Collini J 2019 *Phys. Rev. Lett.* **122** 147601
[12] Kudo K, Takasuga M, Okamoto Y, Hiroi Z and Nohara M 2012 *Phys. Rev. Lett.* **109** 097002
[13] Pavlov N S, Kim T K, Yaresko A, Choi K Y, Nekrasov I A and Evtushinsky D V 2021 *J. Phys. Chem. C* **125** 28075
[14] Kurita N, Ronning F, Tokiwa Y, Bauer E D, Subedi A, Singh D J, Thompson J and Movshovich R 2009 *Phys. Rev. Lett.* **102** 147004
[15] Subedi A and Singh D J 2008 *Phys. Rev. B* **78** 132511

[16] Lederer S, Schattner Y, Berg E and Kivelson S A 2015 *Phys. Rev. Lett.* **114** 097001

[17] Lederer S, Berg E and Kim E A 2020 *Phys. Rev. Res.* **2** 023122

[18] Song L, Si J, Fennell T, Stuhr U, Deng G, Wang J, Liu J, Hao L, Luo H, Liu M and Li S 2024 *Phys. Rev. B* **109** 104518

[19] Qin T, Zhong R, Cao W, Shen S, Wen C, Qi Y and Yan S 2023 *Nano Lett.* **23** 2958

[20] Ronning F, Kurita N, Bauer E, Scott B, Park T, Klimczuk T, Movshovich R and Thompson J D 2008 *J. Phys.: Condens. Matter* **20** 342203

[21] Chen Z, Xu G, Hu W, Zhang X, Zheng P, Chen G, Luo J, Fang Z and Wang N 2009 *Phys. Rev. B* **80** 094506

[22] Liang Z W, Hou X Y, Zhang F, Ma W R, Wu P, Zhang Z Y, Yu F H, Ying J J, Jiang K, Shan L, Wang Z Y and Chen X H 2021 *Phys. Rev. X* **11** 031026

[23] Li A, Yin J X, Wang J, Wu Z, Ma J, Sefat A S, Sales B C, Mandrus D G, McGuire M A and Jin R 2019 *Phys. Rev. B* **99** 134520

[24] Dynes R, Garno J, Hertel G and Orlando T 1984 *Phys. Rev. Lett.* **53** 2437

[25] Bardeen J, Cooper L N and Schrieffer J R 1957 *Phys. Rev.* **108** 1175

[26] Eliashberg G 1960 *Sov. Phys. JETP* **11** 696

[27] Schrieffer J, Scalapino D J and Wilkins J 1963 *Phys. Rev. Lett.* **10** 336

[28] McMillan W and Rowell J 1965 *Phys. Rev. Lett.* **14** 108

[29] Shan L, Gong J, Wang Y L, Shen B, Hou X Y, Ren C, Li C H, Yang H, Wen H H, Li S L and Dai P 2012 *Phys. Rev. Lett.* **108** 227002

[30] Moore S A F J, Iavarone M 2015 *Supercon. Sci. Technol.* **28** 045003

[31] Hess H, Robinson R and Waszczak J 1990 *Phys. Rev. Lett.* **64** 2711

[32] Caroli C, De Gennes P and Matricon J 1964 *Phys. Lett.* **9** 307

[33] Renner C, Kent A, Niedermann P, Fischer Ø and Lévy F 1991 *Phys. Rev. Lett.* **67** 1650

[34] Lechner E M, Oli B D, Makita J, Ciovati G, Gurevich A and Iavarone M 2020 *Phys. Rev. Appl.* **13** 044044

[35] Fang D, Yang H and Wen H H 2023 *Sci. Sin. Phys. Mech. Astron.* **53** 127404

[36] Kogan V and Zhelezina N 2005 *Phys. Rev. B* **71** 134505

[37] Narayan D M, Hao P, Kurleto R, Berggren B S, Linn A G, Eckberg C, Saraf P, Collini J, Zavalij P and Hashimoto M 2023 *Sci. Adv.* **9** eadi4966

[38] Dagan Y, Beck R and Greene R L 2007 *Phys. Rev. Lett.* **99** 147004